Disappearance and reappearance of magnetic ordering upon lanthanide substitution in $(Er_{1-x}Dy_x)Al_2$

A. L. Lima,[1] K. A. Gschneidner, Jr.,[1,2,*] V. K. Pecharsky,[1,2] and A. O. Pecharsky[1]
[1]*Ames Laboratory, Iowa State University, Ames, Iowa 50011-3020, USA*
[2]*Department of Materials Science and Engineering, Iowa State University, Ames, Iowa 50011-3020, USA*
(Received 30 April 2003; published 7 October 2003)

Multiple magnetic ordering phenomena, when substituting Dy for Er in $(Er_{1-x}Dy_x)Al_2$ over a broad range of concentrations $0 \leqslant x \leqslant 0.85$, observed in low-temperature heat capacity measurements have been explained theoretically. The Hamiltonian that describes the system includes crystalline electric field effects, exchange interaction, and second-order contributions such as quadrupolar and magnetoelastic effects. We show that the discontinuity in the heat capacity, which arises at certain concentrations of the alloying element Dy, is the result of the competition between the magnetoelastic coupling and quadrupolar effects. The existence of the disappearance and reappearance of the magnetic phases in other lanthanide-lanthanide systems is also discussed.

DOI: 10.1103/PhysRevB.68.134409 PACS number(s): 75.10.Dg, 71.20.Lp, 74.25.Ha, 75.30.Sg

INTRODUCTION

In the past ten years, there has been a growing interest in the use of magnetic materials for cooling applications.[1,2] Lanthanide compounds and alloys, which magnetically order below 20 K and have large magnetic heat capacities, are already employed as cryocooler regenerator materials to cool down to 4 K,[1] while lanthanide materials which order ferromagnetically near room temperature are being considered for their magnetocaloric properties as active magnetic regenerator (AMR) materials for near-room-temperature refrigeration and cooling.[2] In many cases, it is necessary to adjust the magnetic ordering temperature of a material to make optimum use of its magnetothermal properties. One of the best ways to do this is to partly substitute one lanthanide element for another one to attain the desired ordering temperature.[1,3] In our investigation to increase the low-temperature (<20 K) heat capacity of Er metal as a cryocooler regenerator material, Pr was found to be an effective alloying agent.[1] Another study to find an inexpensive and improved AMR material for hydrogen liquefaction involved the $(Er_{1-x}Dy_x)Al_2$ system.[4,5] In both of these studies it was found that the low-temperature magnetic ordering [the transition below the upper Néel (Er) or Curie ($ErAl_2$) temperature] of the the Er-based material (i.e., pure Er and $ErAl_2$, respectively) disappeared upon alloying Pr and Dy, respectively, but as more Pr (or Dy) was added, an apparent new magnetic phase appeared, which in turn vanished upon further alloying; and finally, yet another new magnetic phase was observed at even higher concentrations of the alloying element (see Refs. 1 and 6 for the $Er_{1-x}Pr_x$ alloys and Ref. 5 for $Er_{1-x}Dy_xAl_2$ alloys). We have called these unusual behaviors the ''DADA'' (disappearance, appearance, disappearance, appearance) phenomena. As far as we are aware the DADA behavior has not heretofore been observed.

In order to understand the DADA behavior we have carried out crystalline electric field (CEF) calculations including second-order effects such as quadrupole interations, for the $(Er_{1-x}Dy_x)Al_2$ system. The CEF effects are already well described in the literature for the binary RAl_2 phases:[7] however, there are other interactions affecting the lanthanide ions which are often, but should not be always, neglected. Certainly, the quadrupolar interactions are among the most important second-order effects. The quadrupolar interactions consist of two contributions: one is related to the coupling of spins. A biquadratic coupling between the spins leads to quadrupolar exchange due to indirect Coulomb and exchange interactions, where conduction electrons may play an important role.[8] The second contribution from the quadrupolar effect is that the lattice is usually coupled to the quadrupoles in the $4f$ shell, promoting magnetoelastic effects.[9] Some magnetoelastic interactions can be observed as lattice distortions and, therefore, explained by the cooperative Jahn-Teller theory, while others are treated as magnetostrictive effects. As commonly known, the magnetostriction effects, which are isotropic or anisotropic lattice deformations exhibited by a magnetic material when it becomes magnetized as a result of the influence of an applied magnetic field, are present in both $ErAl_2$ and $DyAl_2$.[7] In general, the $4f$ systems are not considered as conventional Jahn-Teller systems; however, the weak vibronic coupling narrows the lines of the optical spectrum, which enables them to be observed with high precision.[10] Nevertheless, the influence of the local Jahn-Teller distortions—namely, the instability of highly symmetric systems as a result of the interaction of degenerated electronic states with another subsystem and the consequent formation of several degenerated low-symmetry configurations of the total system—and the structural phase transition induced by these distortions of the magnetic structure formed below the compound's critical temperature can be visualized in lanthanide compounds.[10] Due to the strong spin-orbit coupling in the lanthanide compounds, the magnetic moment and Jahn-Teller operators are described on the bases of the same electronic states. These two orderings will not coexist: only the one, which leads the system to its lower energy, prevails.

For $ErAl_2$, the magnetoelastic coupling constants were determined by Stanley *et al.*,[11] using magnetostriction measurements in the ferromagnetic phase. Their study, however, shows that the incorporation of the coupling constants into

the mean-field approach would weakly affect the values of fitted crystal field parameters. For $DyAl_2$, the contributions of both magnetostriction and quadrupolar exchange play a more important role in reproducing the discontinuous change in the magnetization along the [111] direction.[7] Moreover, Lima *et al.* investigated $DyAl_2$ single crystal with a magnetic field vector oriented parallel to the three main crystallographic directions [100], [110], and [111] and concluded that spin reorientation is mostly responsible for the unusual features of magnetic and magnetocaloric properties.[12]

In this work, we present some additional experimental measurements taken on alloys near the critical compositions in the DADA sequence and theoretical insight on the changes in the variation of the heat capacity peaks within the series $(Er_{1-x}Dy_x)Al_2$ when x changes from 0 to 0.85. In order to explain the experimentally observed data, we extended a mean-field model[13] and included second-order effects that account for quadrupolar and magnetoelastic effects. Our model explains the observed experimental features and also describes a systematic change in the behavior of the system as a function of the Dy concentration.

EXPERIMENTAL PROCEDURE

Dy and Er metals were obtained from the Materials Preparation Center of the Ames Laboratory. The lanthanides were 99.8+ at. % pure with the following major impurities (in ppm atomic): Dy-H(800), F(690), O(500), N(46), Mn(24), Fe(23), Cl(23), Ta(17), and C(10) and Er-H(828), O(546), F(246), C(97), N(60), Fe(19), Cl(14), Ta(2), and Mn(1). The Al was purchased from a commercial vendor and was reported to be 99.99 wt % pure. The samples were prepared by arc-melting the two lanthanide metals to form the corresponding $Er_{1-x}Dy_x$ alloy, which then were arc-melted with Al to form $(Er_{1-x}Dy_x)Al_2$. Annealing was not necessary since all compounds melt congruently. According to x-ray powder diffraction and optical metallography examinations, the samples were over 99% single phase. The heat capacity was measured in an adiabatic heat-pulse calorimeter[14] in the temperature range from ~3.5 to 350 K at several applied fields ($H=0$, 20, 50, 75, and 100 kOe).

THEORY

The pseudobinary $(Er_{1-x}Dy_x)Al_2$ alloys exhibit a nearly linear increase in the Curie temperatures (T_C) from series extremes $ErAl_2$, $T_C=13.6$ K, to $DyAl_2$, $T_C=63.9$ K,[5] and the peak value of the adiabatic temperature change (see Fig. 7 of Ref. 5) and isothermal magnetic entropy change (see below) as functions of temperature follow a nonlinear decrease with Dy concentration. In particular, the compound $DyAl_2$ has been extensively studied in part due to the success of the RKKY model describing many of its magnetic properties.[15]

Both $ErAl_2$ and $DyAl_2$ crystallize in the cubic $C15$ $MgCu_2$-type Laves phase structure. The point symmetry of the rare earth ion is $\bar{4}3m$, but it lacks a center of inversion. The usual CEF Hamiltonian can still be used. In order to take into account the CEF interaction, exchange interaction, lattice, and electronic contributions, the Hamiltonian to be solved can be written as

$$H=H_{cef}+H_{mag}, \tag{1}$$

where

$$H_{cef}=W\left[\frac{X}{F_4}(O_4^0+5O_4^4)+\frac{(1-|X|)}{F_6}(O_6^0-21O_6^4)\right] \tag{2}$$

and

$$H_{mag}=-g\mu_B[B_m^xJ^x+B_m^yJ^y+B_m^zJ^z]. \tag{3}$$

Equation (2) represents the CEF interaction for an ion in Lea-Leask-Wolf notation,[16] where W is the energy scale of CEF and $X\,(-1<X<1)$ gives the relative importance between the contribution of the fourth- and sixth-order Stevens operators O_n^m. The dimensionless constants F_4 and F_6 have the values 60 and 13 862, respectively,[16] and g is the Landé factor. Moreover, Eq. (3) describes the Zeeman effect and B, the effective magnetic field experienced by the system, is given by the molecular field approximation as

$$B_m^n=B_0\cos(\phi)+\lambda M^n \quad \text{for} \quad n=x,y,z \quad \text{and} \quad \phi=\alpha,\beta,\gamma, \tag{4}$$

where B_0 is the applied field, M^n is the magnetization calculated using an extended Bak model,[17] and λ is the exchange parameter. The cosines are the direction cosines for the three crystallographic axes. The CEF parameters λ and g are considered to be linear functions of the concentration, and the input values for the series end members $DyAl_2$ and $ErAl_2$ were taken from the literature.[13]

In a mean-field approximation, the biquadratic exchange interaction, as given by Purwins and Leson,[7] can be described by

$$H_Q=-K_1(\langle O_2^0\rangle O_2^0+3\langle O_2^2\rangle O_2^2)-4K_2(\langle P_{xy}\rangle P_{xy}+\langle P_{yz}\rangle P_{yz}+\langle P_{zx}\rangle P_{zx}), \tag{5}$$

where O_2^0, O_2^2, and P_{ij} for $i,j=x,y,z$, the combination of the angular momentum operator, are the Stevens equivalent operators of the second order, and K_1 and K_2 are the biquadratic coupling constants. In order to evaluate the magnetoeslastic interaction, we adopt a general expression for a cubic ferromagnet:[18]

$$H_{mel}=-B_1(\varepsilon_3O_2^0+\sqrt{3}\varepsilon_2O_2^0)-B_2(\varepsilon_{xy}P_{xy}+\varepsilon_{yz}P_{yz}+\varepsilon_{zx}P_{zx}), \tag{6}$$

where B_1 and B_2 are the magnetoelastic coupling constants and $\varepsilon_{i,j}$ are the symmetrized external strain modes adapted to cubic symmetry. The two contributions can be combined to reach the final expression

$$H_{Q+mel}=-G_1(\langle O_2^0\rangle O_2^0+3\langle O_2^2\rangle O_2^2)-G_2(\langle P_{xy}\rangle P_{xy}+\langle P_{yz}\rangle P_{yz}+\langle P_{zx}\rangle P_{zx}), \tag{7}$$

where G_1 and G_2 are constants. For $(Er_{1-x}Dy_x)Al_2$ alloys, $G_1=0.000\,088$ meV and $G_2=-0.0023$ meV.

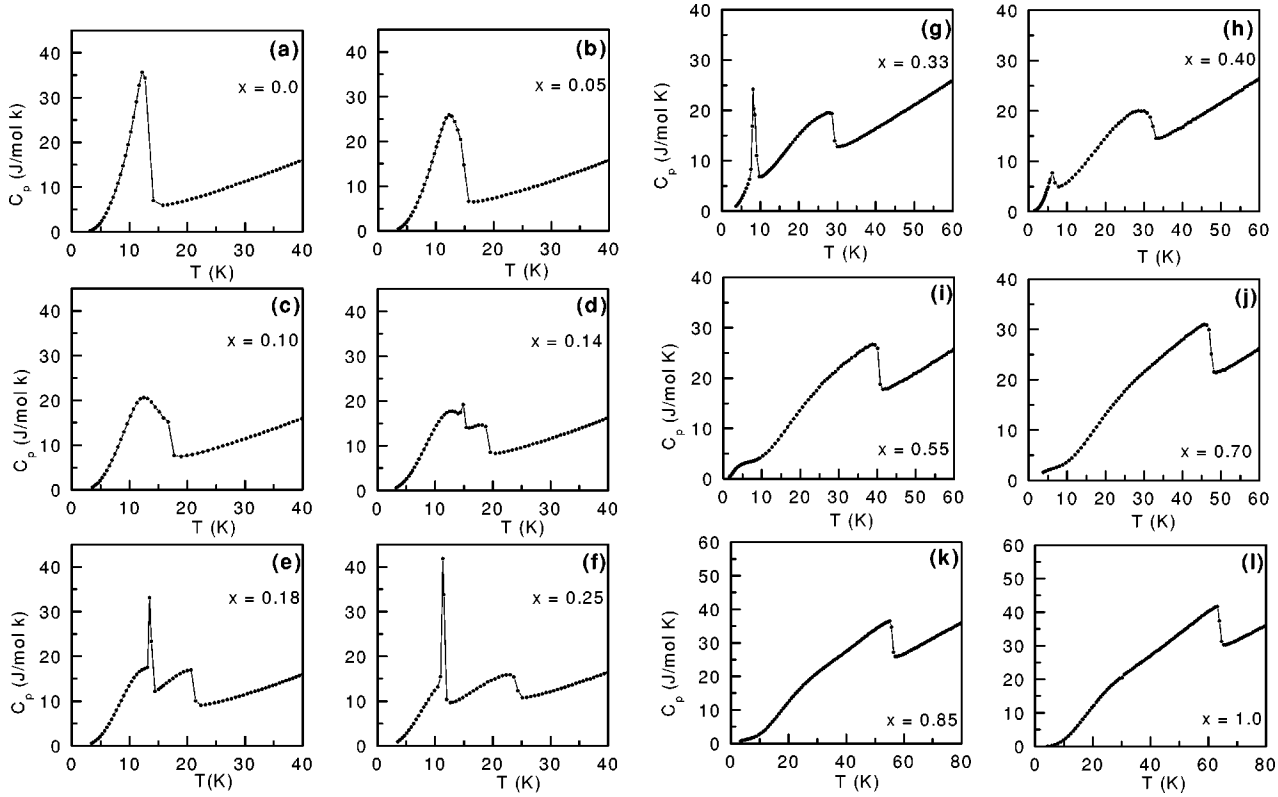

FIG. 1. The zero-magnetic-field heat capacity of the $(Er_{1-x}Dy_x)Al_2$ alloys: (a) $ErAl_2$, (b) $(Er_{0.95}Dy_{0.05})Al_2$, (c) $(Er_{0.90}Dy_{0.10})Al_2$, (d) $(Er_{0.86}Dy_{0.14})Al_2$, (e) $(Er_{0.82}Dy_{0.18})Al_2$, (f) $(Er_{0.75}Dy_{0.25})Al_2$, (g) $(Er_{0.67}Dy_{0.33})Al_2$, (h) $(Er_{0.6}Dy_{0.4})Al_2$, (i) $(Er_{0.45}Dy_{0.55})Al_2$, (j) $(Er_{0.30}Dy_{0.70})Al_2$, (k) $(Er_{0.15}Dy_{0.85})Al_2$, and (l) $DyAl_2$.

Thus, the total Hamiltonian that describes the system is

$$H = H_{mag} + H_{cef} + H_{Q+mel}. \tag{8}$$

As Eq. (8) is solved, we calculate the partition function and then obtain all other quantities such as magnetization, free energy, entropy, etc. In order to calculate the total entropy correctly, we have to include the lattice and electronic contributions as follows and as shown in Ref. 13:

$$S_T(B,T) = S_{mag}(B,T) + S_{latt}(T) + S_{el}(T), \tag{9}$$

where the magnetic contribution is given by

$$\mu_0\left(\frac{\partial S_M}{\partial B}\right)_T = \left(\frac{\partial M}{\partial T}\right)_B, \tag{10}$$

where the magnetization M is obtained from a self-consistent solution of the magnetic state equation. The lattice contribution is obtained from

$$S_{latt} = -3R\ln\left[1-\exp\left(\frac{\Theta_D}{T}\right)\right] + 12R\left(\frac{T}{\Theta_D}\right)^3\int_0^{\Theta D/T}\frac{x^3dx}{\exp(x)-1}, \tag{11}$$

and, finally, the electronic contribution is calculated by

$$S_{el} = \gamma T. \tag{12}$$

We also include a self-consistent procedure for all expected values of the operators P_{ij} and O_2^i (heretofore called second-order operators) and a minimization of the energy to allow the spin rotation according to the magnetic phase diagram.[5] For clarity, we will simply call O_2^i quadrupolar operators and P_{ij} magnetoelastic operators, so that we can analyze and compare the different contribution of each term. Since our samples are polycrystalline, we adopted an average over the three crystallographic directions [100], [110], and [111] in order to compare the theoretical results with the measurements.

RESULTS AND DISCUSSION

In the $(Er_{1-x}Dy_x)Al_2$ system [see Figs. 1(a)–1(l)], as Dy is substituted for Er, the sharp λ-type second-order magnetic heat capacity peak, i.e., at the Curie temperature, of pure $ErAl_2$ (labeled peak *A*) [Fig. 1(a)] gradually broadens [Fig. 1(b)] and changes to a rounded second-order peak (peak *B*), and at the same time the upper Curie temperature peak (T_C) appears as the nearly vertical slope line on the high-temperature side of the heat capacity peak at $x=0.1$ [Fig. 1(c)]. As more Dy is added ($x=0.14$), a sharp peak begins to develop (peak *C*) which coexists with peak *B* [see Fig. 1(d)]. The two peaks (*B* and *C*) still coexist at $x=0.18$ [Fig. 1(e)] but peak *B* becomes weaker and peak *C* is much stronger. At $x=0.25$ [Fig. 1(f)] peak *B* is no longer evident and peak *C* is now fully developed as a narrow peak, which is indicative of

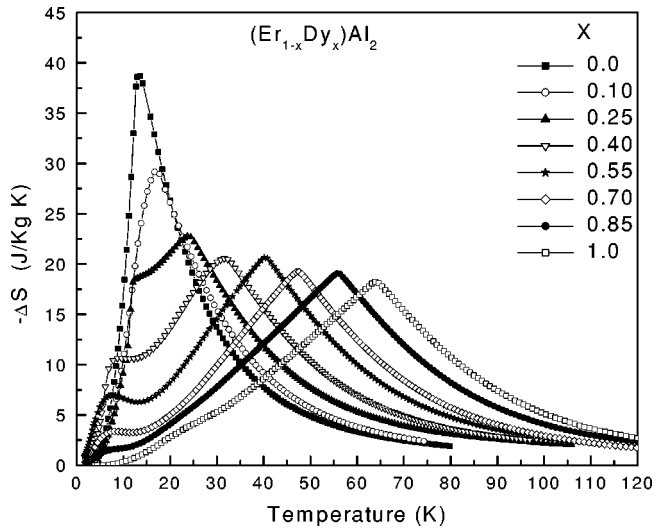

FIG. 2. The magnetocaloric effect in terms of the isothermal magnetic entropy change vs temperature for the $(Er_{1-x}Dy_x)Al_2$ alloys as calculated from heat capacity for a magnetic field change from 0 to 50 kOe.

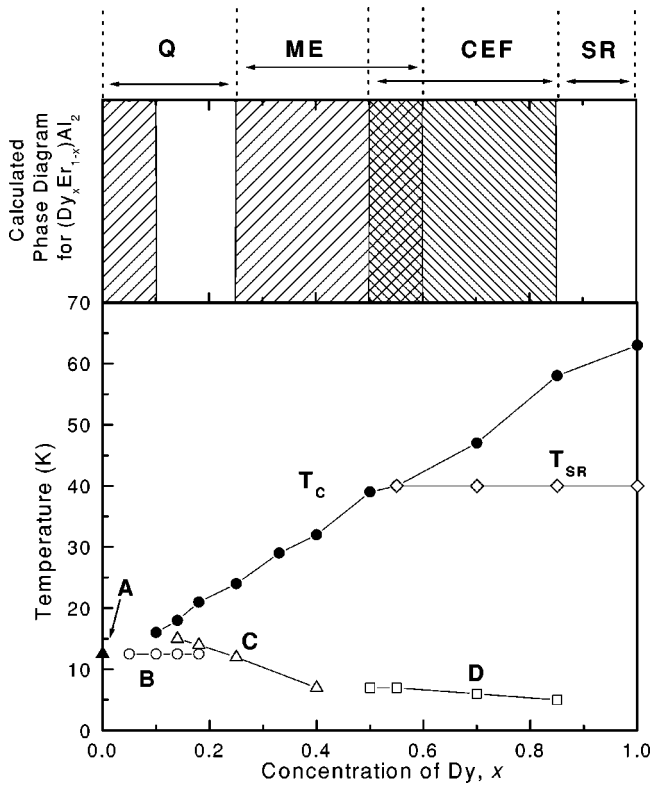

FIG. 3. The various magnetic ordering temperatures as functions of the dysprosium concentration (x). Point A is the sharp heat capacity peak in the pure $ErAl_2$, the points labeled B are the broad rounded heat capacity peaks, the points labeled C are the narrow sharp heat capacity peaks (T_1), the D points are the crystalline electric field peaks, T_C is the Curie temperature, and T_{SR} is the spin reorientation temperature. The calculated phase diagram of $(Er_{1-x}Dy_x)Al_2$ is shown on top and the variously hatched areas indicate the presence of the prevailing contributions. The letters on the top indicate strong contributions to the magnetic energy: ME, magnetoelasticity: Q, quadrupole: CEF, crystalline electric field: and SR, spin reorientation.

a first-order phase transformation. Over the same concentration region, the Curie temperature becomes more evident and shifts to higher temperature with increasing Dy content. As more Dy ($x>0.25$) is added, peak C is retained but its magnitude and temperature are reduced [Figs. 1(g) and 1(h)] and seem to vanish at $x\approx 0.5$ [Figs. 1(h) and 1(i)]. Further Dy additions, $x\geqslant 0.5$, result in another type of magnetic ordering (peak D) at ~ 7 K [Fig. 1(i)] which was thought to be due to CEF effects.[5] This has been recently confirmed by theoretical calculations carried out by Lima *et al.*[13] These broad CEF anomalies are not readily visible in the heat capacity versus temperature plots, but are obvious in the magnetocaloric effect (MCE) parameters—both the adiabatic temperature change ΔT_{ad} (Ref. 5) and the isothermal magnetic entropy change ΔS_M (see Fig. 2)—which are derived from heat capacity measured as a function of temperature and magnetic field.

The location of the upper paramagnetic to ferromagnetic order peak—i.e., the Curie temperature (T_C) for $0.10\leqslant x \leqslant 1.0$—continues to rise in a monotonic linear function as would be expected for the respective de Gennes factor values of Er and Dy [see Figs. 1(c)–1(l) and Fig. 2]. The various transitions as a function of the Dy concentration are plotted in Fig. 3.

Figure 4 presents the comparison between the calculated and measured heat capacity for $ErAl_2$. The theoretical curve reproduces the experimental data quite well. Experimentally the heat capacity of $ErAl_2$ exhibits a sharp peak (peak A) at $T\sim 12$ K while the calculated heat capacity peak is equally sharp with a peak temperature of $T_C\sim 13$ K. The inset shows the contributions of the average second-order terms $\langle O_2^i\rangle$ and $\langle P_{ij}\rangle$ as functions of temperature. For this concentration, the quadrupolar terms O_2^i are negative and smaller in absolute value than the magnetoelastic terms P_{ij}. As seen in the inset of Fig. 4, the second-order terms vanish above T_C.

As more Dy is added, the beginning of the development of peak C for $x=0.14$ is observed [Fig. 1(d)]. Figure 5 is a comparison between the calculated and measured heat capacity as a function of the temperature for $(Er_{0.86}Dy_{0.14})Al_2$. The peak shape of the heat capacity for this composition is different from that calculated for pure $ErAl_2$, $x=0$ (Fig. 4); it is more broad and is consistent with the rounded, broad experimental heat capacity peak. In this case one of the quadrupolar terms dominates and accounts for the broadening of the heat capacity curve. Although the agreement between experiment and theory is not as good as for the pure $ErAl_2$, this difference may be related to some minor contribution(s) neglected in the model. The shape of the curve suggests coexistence of more than one magnetic phase, which is consistent with the development of the sharp peak at ~ 15 K observed experimentally.

In Fig. 6, however, the presence of the new magnetic phase (peak C) is clearly observed in the experimental heat capacity near 10 K for $(Er_{0.75}Dy_{0.25})Al_2$ [Fig. 1(f)]. An ordinary second-order transition occurs, as expected, at the Curie temperature (24 K) where the system goes from a ferromag-

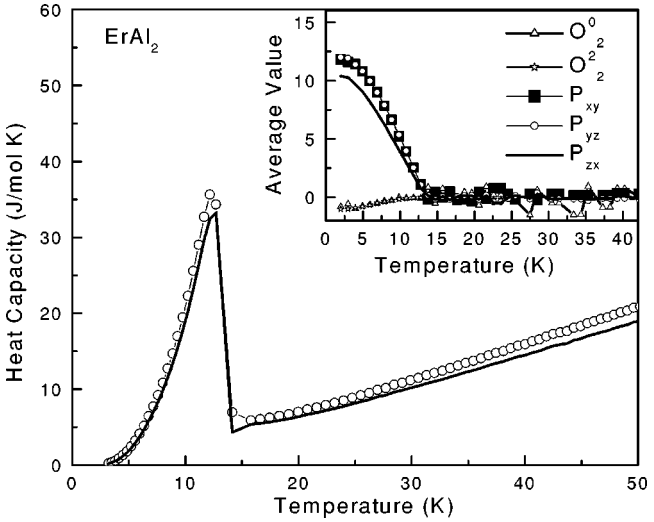

FIG. 4. The measured heat capacity as a function of temperature (open circles) compared to the calculated one (solid line) in zero magnetic field for $ErAl_2$. The inset shows the average values of the second-order terms as functions of temperature where O_i^i are the quadrupole parameters and P_{xy}, P_{yz}, and P_{zx} are the magnetoelastic parameters.

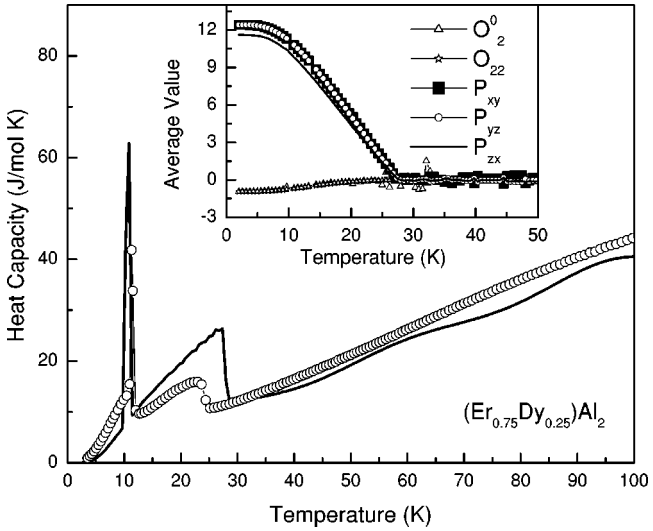

FIG. 6. The measured heat capacity as a function of temperature (open circles) compared to the calculated one (solid line) in zero magnetic field for $x=0.25$. The inset shows the average values of the second-order terms as functions of temperature where O_i^i are the quadrupole parameters and P_{xy}, P_{yz}, and P_{zx} are the magnetoelastic parameters.

netically ordered phase to a paramagnetically disordered one. There is an excellent agreement between the calculated (T_l) and measured temperature (peak C); nevertheless, there is still a displacement of ~ 3 K for the theoretical T_C at ~ 35 K. The inset of Fig. 6 shows the average value of the second-order operators and the same pattern as observed for $ErAl_2$ is repeated: the magnetoelastic coupling is dominant when compared to the quadrupolar effect. Similar to $x=0$ and 0.14, all the second-order contributions vanish above T_C and they are well behaved and continuous functions near T_l. The latter suggests that second-order terms are not directly responsible for the existence of the new magnetic phase, as we will discuss below.

For higher concentrations of Dy, the anomaly at T_l starts to decrease in intensity, but it is still clearly observed experimentally as a sharp peak at ~ 5.7 K in $(Er_{0.6}Dy_{0.4})Al_2$ [see Figs. 1(h) and 7]. The discontinuity (peak C) completely vanishes for $x \geqslant 0.5$ [e.g., see Figs. 1(i)–1(k) and 8 for $x=0.85$]. The second-order terms behave similarly to those for all higher Dy concentrations $0.6 \leqslant x \leqslant 1.0$,: i.e., the qua-

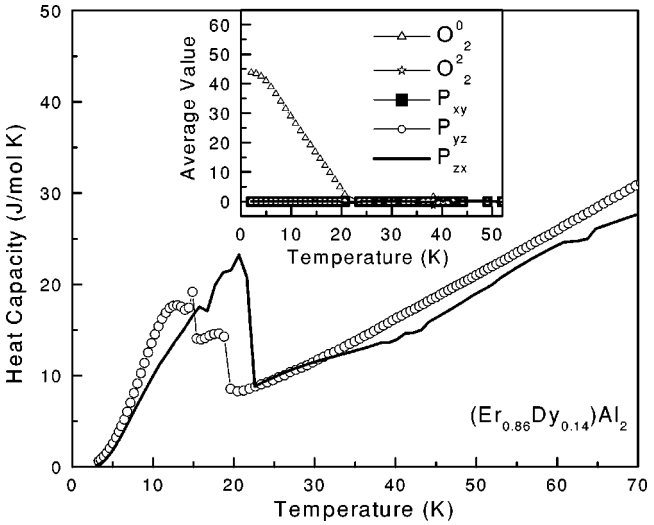

FIG. 5. The measured heat capacity as a function of temperature (open circles) compared to the calculated one (solid line) in zero magnetic field for $x=0.14$. The inset shows the average values of the second-order terms as functions of temperature where O_i^i are the quadrupole parameters and P_{xy}, P_{yz}, and P_{zx} are the magnetoelastic parameters.

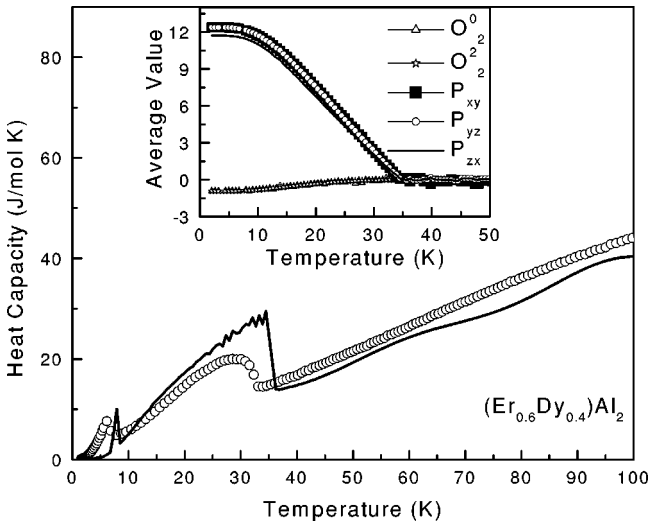

FIG. 7. The measured heat capacity as functions of temperature (open circles) compared to the calculated one (solid line) in zero magnetic field for $x=0.4$. The inset shows the average values of the second-order terms as functions of temperature where O_i^i are the quadrupole parameters and P_{xy}, P_{yz}, and P_{zx} are the magnetoelastic parameters.

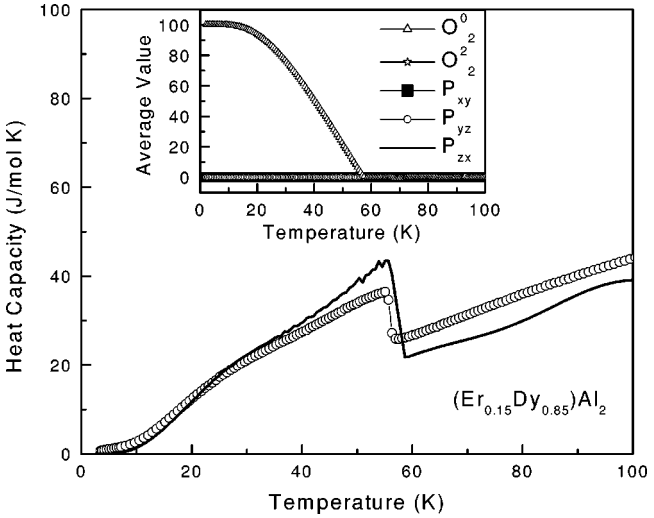

FIG. 8. The measured heat capacity as functions of temperature (open circles) compared to the calculated one (solid line) in zero magnetic field for $x=0.85$. The inset shows the average values of the second-order terms as functions of temperature where O_i^i are the quadrupole parameters and P_{xy}, P_{yz}, and P_{zx} are the magnetoelastic parameters.

drupolar effects prevail over the magnetoelastic coupling. Indeed, in $(Er_{0.15}Dy_{0.85})Al_2$ only one of the quadrupole terms remains nonzero (see Fig. 8).

For the pure $DyAl_2$ (see Fig. 9), there are two possible theoretical approaches to describe its magnetic properties: one includes only the spin reorientation (solid line) and the other includes the second-order effects (dash-dotted line). As we can see, the first approach reproduces the experimental results better. The reasons why it happens may be related to

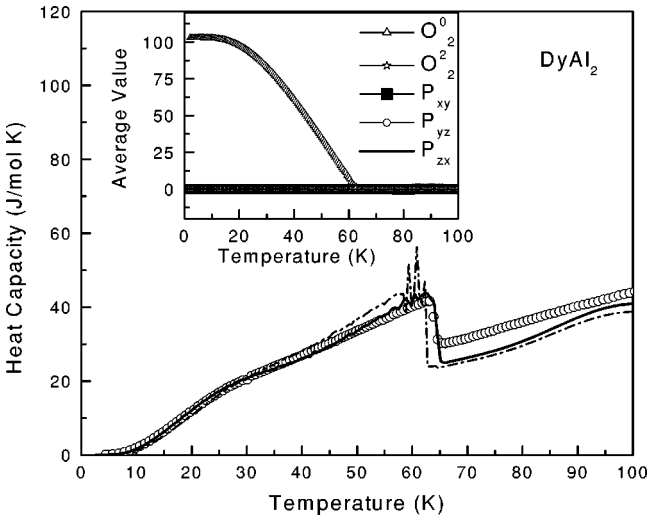

FIG. 9. The zero-magnetic-field measured heat capacity of $DyAl_2$ as a function of temperature (open circles) compared to the calculated one which includes spin reorientation (solid line) and for one which includes the second-order terms (dash-dotted line). The inset shows the average values of the second-order terms as functions of temperature where O_i^i are the quadrupole parameters and P_{xy}, P_{yz}, and P_{zx} are the magnetoelastic parameters.

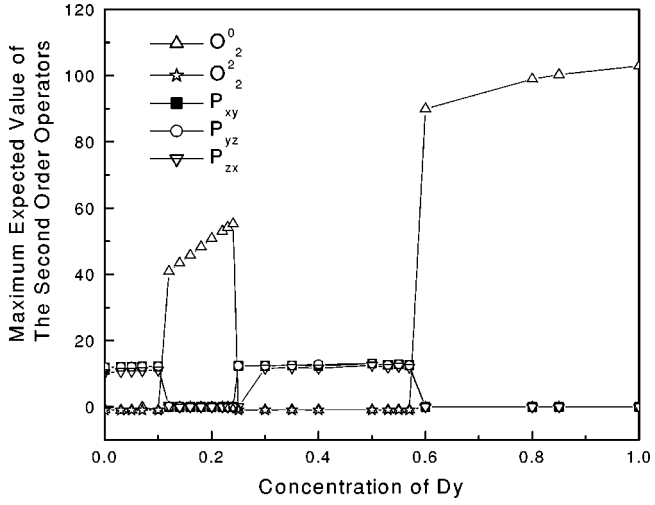

FIG. 10. The maximum average value of the second-order terms as functions of concentration of Dy, where O_i^i are the quadrupole parameters and P_{xy}, P_{yz}, and P_{zx} are the magnetoelastic parameters.

both the choice we made for the input CEF parameters and the stronger contribution of the spin reorientation energy over the second-order terms. In general, for higher concentrations of Dy, the agreement between the experimental and theoretical T_C is better. In terms of theory, it would be possible to improve this agreement for any concentration by choosing another λ input or simply by fixing a value for λ; however, arbitrarily changing the value of the exchange parameter would lead to a solution without the low-temperature anomaly. Our results for pure polycrystalline $DyAl_2$ are in agreement with the values for single-crystal $DyAl_2$.[12] For the single crystal, the model, which includes only the spin reorientation, reproduces the observed features of the magnetocaloric properties.

Figure 10 shows the behavior of the maximum average value of the second-order operators as a function of the Dy concentration. The appearance of peak C without the coexistence of peak B at $x\approx0.25$ and its (peak C) disappearance at $x\approx0.55$ is reproduced theoretically. As long as the magnetoelastic coupling is stronger than quadrupolar effects, these sharp heat capacity peaks are observed experimentally. In other words, the quadrupolar effect does not contribute to the development of the sharp heat capacity peaks A and C, but does lead to the broad-rounded heat-capacity-type peaks (peak B). Moreover, the quadrupolar effect is amplified by the spin reorientation of Dy. Also consistent with these observations (correlations) is the fact that the magnetoelastic parameters for pure $ErAl_2$ are nonzero (Fig. 10) and they account for the sharp heat capacity peak [Fig. 1(a)]. One important indication that the heat capacity discontinuity is related to spin-lattice coupling effects is that the behavior of $(-\Delta S_M)$ versus temperature remains effectively unaltered as we introduce the terms described in Eq. (7). Another indication is that the presence of the sharp peaks is sensitive to the exchange parameter values which, in principle, should be connected only to the value of the T_C. We note that the sharp peak C in the heat capacity coexists with the broad peak B at

$x \approx 0.14$ and $x \approx 0.18$ [Figs. 1(d) and 1(e)], but in this region the quadrupolar contributions prevail over the magnetoelastic ones. This difference between theory and experiment is acceptable and may be associated with the imprecise exchange parameter λ, as mentioned previously, or possibly some other minor contribution to the magnetic energy, which have not been considered. Small discrepancies between theory and experiment may be also related to a nonlinear combination of contributions computed along different crystallographic directions.

Although in pure $DyAl_2$ we do not observe anomalies in the heat capacity below T_C and there is no significant contribution of the second-order parameters to their magnetic and magnetocaloric properties, both are important in explaining the observed behavior in the ternary $(Er_{1-x}Dy_x)Al_2$ alloys. This evidence suggests that the presence of Dy dopping in $ErAl_2$ generates strong magnetoelastic and quadrupolar effects. The result of the CEF effect on the magnetocaloric properties is an observed anomaly in the $(-\Delta S_M)$ vs T in $(Er_{1-x}Dy_x)Al_2$ for $0.5 \leqslant x \leqslant 0.85$: see Fig. 2. This peak in the magnetocaloric effect was theoretically explained to be associated with values of the CEF parameters for which the density of the states of Γ_8^3 presents a peak.[13] The degeneracency of the ground state, Γ_8^3 (quadruplet), is removed in the presence of a molecular field; however, the splitting is not equally spaced. In our model, the CEF parameters are closely related to the concentration of the Dy in $(Er_{1-x}Dy_x)Al_2$; thus, both the CEF effects (without second-order effects) and the CEF effects plus biquadratic coupling (magnetoelastic + quadrupolar) are present depending on the concentration. For high concentrations of Dy, the pure CEF is the dominant effect leading to an anomalous magnetocaloric peak at 7 K. On the other hand, for low concentrations of Dy, the second-order effects may cause a sharp peak in the heat capacity. Indeed, the various peaks shapes in the heat capacity are the results of competition between the magnetoelastic coupling and quadrupolar effects. As expected the sharp heat capacity peaks and the anomaly in $(-\Delta S_M)$ vs T may exist in the concentration range $0.5 \leqslant x \leqslant 0.6$; however, none of them have been observed experimentally, and this may be due to the fact that the low-temperature limit of our calorimeter is 3.5 K and that the T_1 temperatures are less than 3.5 K for these values of x which seems plausible considering the values and the slope of the C peaks versus composition curve shown in Fig. 3 when extrapolated to $0.5 \leqslant x \leqslant 0.6$.

CONCLUSIONS

Mean-field theory has been proved to be a good approach to describe the anomalous behavior of lanthanide compounds. We investigated the origin of the DADA phenomena which is evident in the heat capacity data of $(Er_{1-x}Dy_x)Al_2$ in the $0.0 \leqslant x \leqslant 0.85$ range of concentrations. The presence of quadrupolar and magnetoelastic effects explains the observed behavior of the heat capacity. When the magnetoelastic terms dominate, sharp heat capacity peaks are calculated and observed, while when the quadrupolar terms dominate, rounded-broad heat capacity magnetic ordering peaks are calculated and observed. However, neither of the two contributions seems to have an important role in defining the shape of $(-\Delta S_M)$ versus temperature curve.

The DADA phenomena have also been observed in the heat capacity study of the Er_xPr_{1-x} system,[6] but apparently not in other Er-based systems. Since these phenomena are difficult to detect by using the standard magnetic susceptibility and magnetization measurements, this probably explains why the DADA phenomena have not been observed in studies of lanthanide doping of the other Er-based systems—e.g., the Er-R intralanthanide alloys. It would be interesting to make heat capacity study of $Er_{1-x}Dy_x$ to see what happens to the Er magnetic phase transitions when doped with Dy. The next question we ask ourselves is, does the DADA phenomena exist in other lanthanide-based materials or is it an exclusively limited to Er-based materials because of erbium unique energy level and the influence of the various crystal field environments upon them?

Neutron scattering experiments would be quite useful in elucidating the various magnetic structures and behaviors associated with DADA phenomena described above in the $(Er_{1-x}Dy_x)Al_2$ system.

ACKNOWLEDGMENTS

This paper has been authored by Iowa State University of Science and Technology under Contract No. W-705-ENG-82 with the U.S. Department of Energy. This research was supported by the Office of Basic Energy Sciences, Material Sciences Division of the U.S. DOE. One of us (A.L.L.) acknowledges financial support from CNPq–Conselho Nacional de Desenvolvimento Científico e Tecnológico (Brazil).

*Corresponding author. FAX: 515-294-9579. Electronic address: cagey@ameslab.gov

[1] K. A. Gschneidner, Jr., A. O. Pecharsky, and V. K. Pecharsky, in *Cryoolers 11*, edited by R. S. Ross, Jr. (Kluwer Academic/Plenum, New York, 2001), p. 433.

[2] C. Zimm, A. Jastrab, A. Sternberg, V. K. Pecharsky, K. A. Gschneidner, Jr., M. Osborne, and I. Anderson, Adv. Cryog. Eng. **43**, 1759 (1998).

[3] K. A. Gschneidner, Jr. and V. K. Pecharsky, in *Rare Earth: Science, Technology and Application III*, edited by R. S. Bautista, C. O. Bounds, T. W. Ellis, and B. T. Kilbourn (The Minerals, Metals and Materials Society, Warrendale, PA, 1997), p. 209.

[4] K. A. Gschneidner, Jr., H. Takeya, J. O. Moorman, and V. K. Pecharsky, Appl. Phys. Lett. **64**, 253 (1994).

[5] V. K. Pecharsky, K. A. Gschneidner, Jr., and S. Malik, Adv. Cryog. Eng. **42**, 475 (1996).

[6] K. A. Gschneidner, Jr., A. O. Pecharsky, Y. L. Wu, and V. K. Pecharsky, J. Solid State Chem. **171**, 324 (2003).

[7] H.-G. Purwins and A. Leson, Adv. Phys. **39**, 309 (1990).

[8] S. M. Schmitt and P. M. Levy, J. Magn. Magn. Mater. **50**, 147 (1985).

[9] G. A. Gehring and K. A. Gehring, Rep. Prog. Phys. **38**, 1 (1975).

[10] M. D. Kaplan and B. G. Vekhter, *Cooperative Phenomena in Jahn-Teller Crystals* (Plenum Press, New York, 1995), Chap. 4.

[11] H. B. Stanley, B. D. Rainford, W. G. Stirling, and J. S. Abell, Physica B **130**, 355 (1985).
[12] A. L. Lima, A. O. Pecharsky, V. K. Pecharsky, and K. A. Gschneidner, Jr. (unpublished).
[13] A. L. Lima, I. S. Oliveira, A. Gomes, and P. J. von Ranke, Phys. Rev. B **79**, 172411 (2002).
[14] V. K. Pecharsky, J. O. Moorman, and K. A. Gschneidner, Jr., Rev. Sci. Instrum. **68**, 4196 (1997).
[15] P. M. Gehing, M. B. Salamon, A. del Moral, and J. J. Arnaudas, Phys. Rev. B **41**, 9134 (1990).
[16] K. R. Lea, M. J. Leask, and W. P. Wolf, J. Phys. Chem. Solids **23**, 1381 (1962).
[17] A. L. Lima, P. J. von Ranke, A. M. Gomes, A. Y. Takeuchi, A. P. Gimarães, and I. S. Oliveira, J. Alloys Compd. **344**, 375 (2002).
[18] A. del Moral and M. S. S. Brooks, J. Phys. C **7**, 2540 (1974).